J Mater Sci (2015) 50:6578–6585
DOI 10.1007/s10853-015-9199-2

Novel felt pseudocapacitor based on carbon nanotube/metal oxides

Derrick W. H. Fam[1] · Sue Azoubel[2] · Liang Liu[1,2] · Jingfeng Huang[1] · Daniel Mandler[2] · Shlomo Magdassi[2] · Alfred I. Y. Tok[1]

Received: 28 January 2015 / Accepted: 22 June 2015 / Published online: 7 July 2015

Abstract This work describes a novel supercapacitor electrode based on a glass fiber felt substrate, single-walled carbon nanotube (SWCNT) and metal oxide layers (RuO_2 or MnO_2). It is fabricated by the repeated and alternate deposition of SWCNTs and metal oxides via dipping and electrodeposition, respectively, to achieve three-dimensional layered hierarchical structured supercapacitor electrodes. The results show that the layered structured electrodes fabricated by alternating deposition of SWCNTs and metal oxides have higher capacitance as compared with the bulk deposited samples, which are fabricated by deposition of SWCNTs followed by metal oxides. The best configuration studied in this work shows specific capacitance of 72 and 98 F/g for the SWCNT–MnO_2 and SWCNT–RuO_2, respectively, whereas the corresponding areal capacitances are 0.07 and 0.09 F/cm^2. This three-dimensional porous electrode structure design combines the high mechanical stability of the felt substrate with the high conductivity and specific surface area of SWCNTs, and the high capacitance of metal oxides. This will add immensely to the research and development of wearable lightweight electronics in harsh environments.

✉ Alfred I. Y. Tok
miytok@ntu.edu.sg

[1] School of Materials Science and Engineering, Nanyang Technological University, Singapore 639798, Singapore

[2] Institute of Chemistry, The Hebrew University of Jerusalem, 9190401 Jerusalem, Israel

Introduction

The advent of nanotechnology opens up the potential for miniaturizing electronic components thereby paving the way for the fabrication of portable, flexible yet high-performance electronic devices that has many applications such as in electric or hybrid vehicles, printed electronics, and also in the aerospace industry. However, one of the major challenges is in fabricating suitable power sources that are compatible with these devices. Therefore, state-of-the-art energy storage devices, such as highly efficient batteries and capacitors, are the focus of substantial research efforts. Conventional supercapacitors are characterized by their high power density but have a relatively low energy density. This is because they function solely through charging the surface of the electrode forming an electric double layer (EDL). Therefore, electrodes based on conducting nanomaterials having higher surface area in contact with the electrolyte would result in higher capacitance. Another type of supercapacitors, termed pseudocapacitors, combines the EDL effect with charge stored through reversible redox reactions occurring at the surface of the electrodes. This is usually achieved by combining redox materials, e.g., conductive polymers [1–5] and transition metal oxides [6–10], with the conducting electrodes. Pseudocapacitors have attracted much attention due to their ability to combine the charge storage capability of batteries and the high power density of conventional capacitors.

The discovery of carbon nanotubes (CNTs) provided the impetus for current advancements in various fields including charge storage technologies [11, 12]. Specifically, single-walled CNTs (SWCNTs) exhibit very high theoretical specific surface area of 1315 m^2/g [13] as compared with commercially available activated carbon

(660 m^2/g [14]), making it a conductive material that is highly desired in supercapacitors. CNTs are also known for high tensile strength [15], which makes them viable as a material for flexible integrated electronics.

CNTs have been extensively used for assembling supercapacitors. This area has been reviewed by Bose [16] and Pan [17], which includes a wide variety of materials combined with different types of CNTs, i.e., SWCNTs and multi-walled CNTs (MWCNTs). However, the specific capacitance reported of similar systems span over a wide range of values, which indicates of the uncertainty of measurement that is mostly due to the error in weighing the active materials as regular lab balances do not have high enough resolution. At the same time, for practical applications, the areal capacitance, which is often neglected in the reported data, should also be considered.

Among the metal oxides to be coupled with CNTs, RuO_2 and MnO_2 are considered to be the most promising. The former has fairly high conductivity, redox reversibility, and stability in various electrolytes [18–22], and the latter has low cost and relatively comparable properties. In a recent study, RuO_2 and MnO_2 were deposited on carbon fabric from Ru(VII) and Mn(VII) solutions, respectively [18]. The deposition was accomplished by soaking in solutions of $KRuO_4$ and $KMnO_4$ for several hours. The morphology of the resultant oxide films showed very little cracks, especially for the MnO_2 samples. This report also showed that RuO_2 and MnO_2 possess high capacities of ca. 824 F/g in 1 M H_2SO_4 and 1080 F/g in 2 M LiOH. Furthermore, their ability to be coupled with carbon fabric reveals their possible compatibility with CNTs. However, the total capacitance of this device depended mostly on the reversible redox reactions of the oxides as it covers most parts of the carbon fibers therefore resulting in a device with lower power capabilities on EDL as a charge storage mechanism. Reviewing studies like these reveals that the method of electrode assembly, namely, the approach for mixing CNTs and metal oxides, is still to be optimized. Metal oxides are usually deposited in the CNT network without morphological control in the form of nanoparticles [19, 20, 23], bulk electrochemically deposited films [7, 24, 25], or simply by mixing or forming the metal oxide nanoparticles in the presence of the CNTs [10, 26, 27]. The interfacial assembly and properties of the intimate contact between the two components, i.e., the conductive and the redox materials, are of utmost importance and will affect significantly the total capacitance. However, by coupling these oxides with CNTs, high electrical resistance is introduced and this impedes the charge transfer from the oxides to the CNTs and the current collectors [27]. More importantly, the uncontrolled deposition of the CNTs and the redox materials also reduces the area in which the active material is in contact with the electrolyte. Some strategies explored to mitigate this problem would be the use of electrophoresis [28, 29], dip coating [30], and air-spraying to deposit the active materials [5]. However, most of these techniques are only able to deposit the active material on the surface of the current collector, and thereby, the effective surface area that is available for charge collection is limited to the size of the current collector, and thickness and the porosity of the film. However, these challenges are not reflected if only the specific capacitance values are reported as in most cases. Therefore, a three-dimensional porous structure would be necessary to store a practical amount of charge without the need for a large current collector surface area as the bulk of the material can then be utilized as well.

In this work, a method for assembling of CNTs/metal oxides on a glass fiber felt was demonstrated. The latter was used as a flexible, stable 3D support with high surface area, which is superior as compared with most of the conventional flexible materials such as cellulose and polyester. A three-dimensional hierarchical layered structure was fabricated by sequentially depositing CNTs and metal oxides, i.e., RuO_2 or MnO_2. It was found that the layered hierarchical structure has the potential to enhance the utilization of both the EDL and the pseudocapacitive components as seen in the improvement of the specific and areal capacitance as compared with the bulk architecture.

Experimental

Carboxylic acid-functionalized SWCNTs (P3, 0.5–3 μm in length and 1.4 nm in diameter) were procured from Carbon Solutions, Inc. and used as received. Glass fiber felt (20 μm in diameter of single fiber) was obtained from Hollingsworth and Vose (USA). Ru(III) and Mn(VII) solutions were prepared [18, 31] from $RuCl_3{\cdot}xH_2O$ (Aldrich, ReagentPlus®) and $KMnO_4$ (Merck, EMSURE®ACS), respectively. Ru(III) solution consisted of 5 mM $RuCl_3{\cdot}xH_2O$, 0.1 M NH_4Cl, and 0.01 M HCl, while the Mn(VII) solution contained 20 mM $KMnO_4$, both dissolved in deionized water. Electrodeposition and all electrochemical measurements were carried out in a 3-electrode system using a Pt counter electrode of $10 \times 20 \times 0.2$ mm^3 and an Ag/AgCl reference electrode. The working electrode is the glass felt soaked with SWCNTs, having apparent area of 4.5 cm^2. The depositions of RuO_2 and MnO_2 were both performed using cyclic voltammetry (CV). RuO_2 was deposited from the $RuCl_3$ solution by CV upon scanning the potential between 0.4 and 1.1 V at 50 mV/s. Similarly, MnO_2 was deposited from the $KMnO_4$ solution by cycling the potential between 0.4 and −1.0 V at the same scan rate. Homogeneous aqueous SWCNT suspension of 1 mg/mL was prepared by sonication for 2 h using a probe sonicator. The glass fiber felts were cut into 1.5×3 cm^2 rectangles and immersed in the SWCNT solution for a few seconds and then dried at 120 °C for

6 min. The immersion and drying steps are denoted as a single SWCNT deposition cycle.

Fabrication of the layer-deposited samples comprised an initial stage of 15 SWCNT deposition cycles to assure good conductivity. The weight and conductivity of the SWCNT layer were measured after each cycle. The 15 SWCNT deposition cycles were followed by repeated alternating deposition via 50 CV cycles of oxide (either MnO_2 or RuO_2) and 5 soaking cycles of SWCNT until 150 CV cycles of oxide and 25 deposition cycles of SWCNT in total (15 SWCNT/50 oxide/5 SWCNT/50 oxide/5 SWCNT/50 oxide) as shown in Fig. 1 (from (b) to (g)) were obtained. Fabrication of bulk deposited samples comprised 25 deposition cycles of SWCNTs followed by 150 CV cycles of oxide (25 SWCNT/150 oxide).

Resistivity measurements was obtained using a Jandel-RM3000 test unit and multi-height probe with solid tungsten carbide probe needles at 1 mm linear spacing and 100 g loads. The electrochemical characterization of the samples was carried out by CV in 1 M H_2SO_4 for RuO_2–SWCNT and 1 M Na_2SO_4 for MnO_2–SWCNT samples at 5 mV/s. The electrochemical impedance spectroscopy was measured in 1 M H_2SO_4 solution at open circuit potential in the frequency range of 10^5–10^{-2} Hz, with a sine wave of 10 mV amplitude. Cyclic stability was measured by means of galvanostatic charge/discharge at a current density of 1 A/g from 0 to 0.7 V for all cells. All electrochemical measurements were performed at room temperature (~25 °C) on a Solartron 1400A potentiostat/galvanostat. The morphology of the samples was characterized using the JEOL 7600F field-emission scanning electron microscope (FESEM).

Results and discussion

Before constructing the SWCNT–metal oxide layered assembly, the deposition of multi-layers of SWCNT was studied in order to optimize the weight of SWCNTs to be loaded. The optimal electrode should possess the lowest possible weight and resistivity. Figure 2 shows the effect of loading cycles (up to 30) of SWCNTs on the weight, resistivity, and capacitance of the electrodes. As seen from Fig. 2a, the weight of the SWCNTs increases linearly with the loading cycles, implying an almost constant loading per cycle. Below 10 loading cycles, high resistivity was recorded due to the insufficient conduction pathways. As the SWCNT loading increases, the resistivity decreases. However, as the loading cycles increase beyond 15, the decrease in resistivity is insignificant. This is due to the addition of CNTs which increases the conduction pathway (decreases resistivity) but also adds to the number of nanotube–nanotube junctions (increases resistivity). Figure 2b shows the effect of SWCNT loading on the capacitance of the electrodes. The capacitance of the sample with 5 loading cycles could not be measured due to the poor conductivity of the electrode. Figure 2b shows very clearly that the specific capacitance increases with loading. Considering the specific capacitance, weight, and resistance, the rest of the experiments were carried out applying 15 cycles of SWCNT loaded onto the glass fiber felt as the starting material for the electrodeposition of the oxides because it shows a good compromise between the weight, resistivity, and capacitance of the loaded SWCNTs.

Next, 7 samples of RuO_2 or MnO_2 electrodeposited on the SWCNT were made. From previous reports, it was noted that the performance of MnO_2-based pseudocapacitors does not differ drastically from the RuO_2-based pseudocapacitors at low oxide loading [18, 32, 33], and MnO_2 has lower cost and is more environmental friendly as compared with RuO_2 [32, 34]. Figure 3a shows the specific capacitance of SWCNT–oxide layered electrodes with different loading. Specifically, SWCNT and oxide layers were sequentially deposited as shown in Fig. 1(b)–(g). It is evident that while the specific capacitance of the SWCNT–RuO_2 increases with the loading, that of the SWCNT–

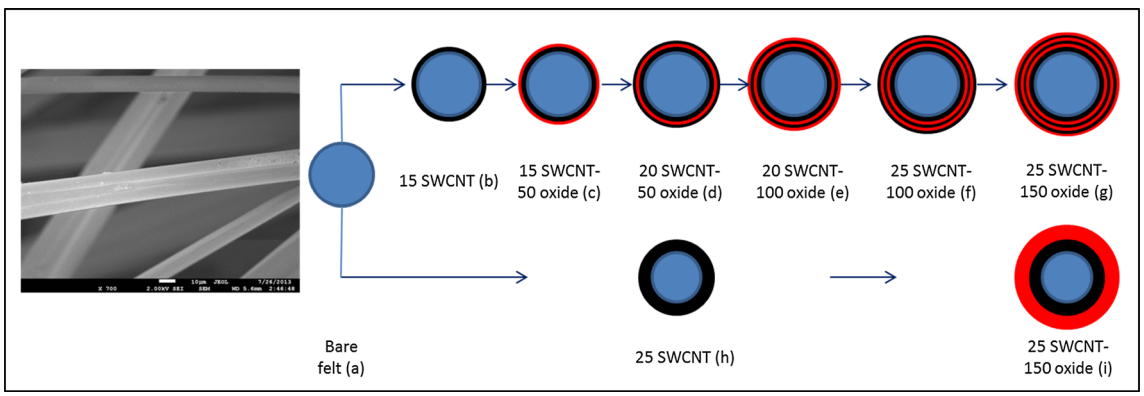

Fig. 1 FESEM image of bare glass fiber and schematic of the layered and bulk deposited structures

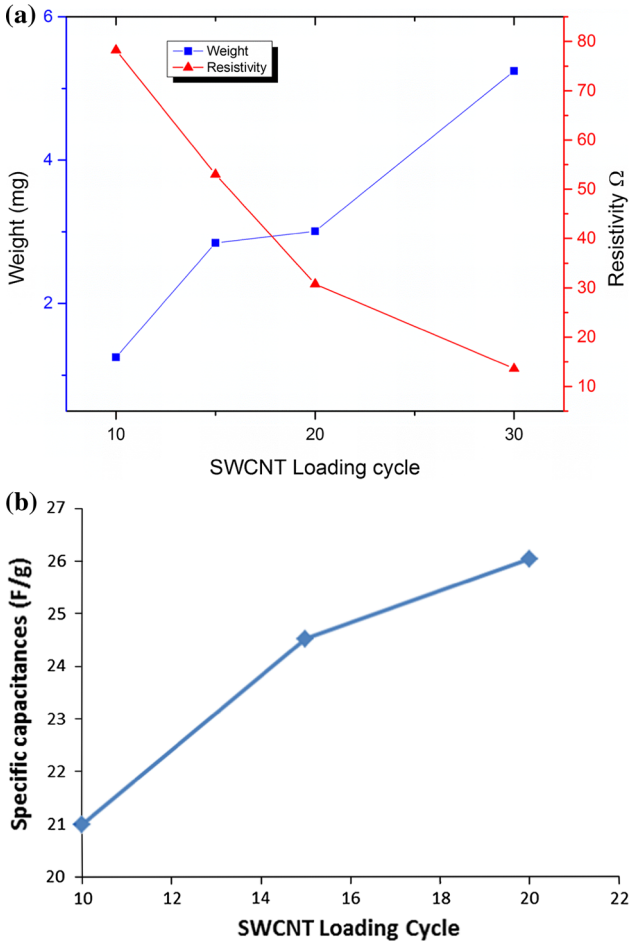

Fig. 2 **a** Resistivity of the electrode and weight of SWCNT as a function of the number of SWCNT loading cycles. **b** Specific capacitances versus the SWCNT loading cycles

MnO_2 levels off after the first oxide deposition (seen in Fig. 3a). This alludes to the difference between the microstructures of the SWCNT–oxides vide infra.

Figure 3b depicts the areal capacitance determined by dividing the actual capacitance with the geometric area ($\sim$4.5 cm^2). Due to the uncertainty in weight measurement as well as the concern for practical usage, the areal capacitance is a more reasonable parameter for comparison. There are three notable observations in Fig. 3b: first, the areal capacitance increases as a result of the first electrodeposition of the oxide as compared with bare SWCNT electrode; second, the capacitance also increases with each of the oxide deposition cycle; third, the difference in capacitance between the two oxides is relatively small. These findings indicate that the electrolyte penetrates across the entire layered structure leading to the increase of capacitance with each layer of oxide deposition. The mean specific capacitances for the best configuration studied [25 layers of SWCNT and 150 electrodeposition cycles of oxide, Fig. 1(g)] for the SWCNT–MnO_2 and SWCNT–RuO_2 are 72 and 98 F/g, whereas the corresponding areal capacitances are 0.07 and 0.09 F/cm^2, respectively.

Further characterization of the electrodes was carried out by CV. Figure 4 shows the CV of SWCNT–oxides. The capacitance of the pseudocapacitors was calculated using the relationship, $C = \frac{\Delta Q}{\Delta V} = \frac{\int_{\text{Lowerhalf}} I dt}{\Delta V}$, where C is the total capacitance, ΔQ is the amount of charge stored, ΔV is the potential window for discharge, and $\int_{\text{Lowerhalf}} I dt$ is the integral of the discharge current with respect to time. The supercapacitors for which the CVs are shown in Fig. 4 were loaded up to 40 wt% of the active material (SWCNTs and oxide) for the MnO_2 samples and about 20 wt% of the active material for the RuO_2 samples at 25 layers of SWCNT and 150 cycles of the respective oxides. It can be seen that the specific current for the SWCNT–RuO_2 samples was higher than that for the SWCNT–MnO_2 samples.

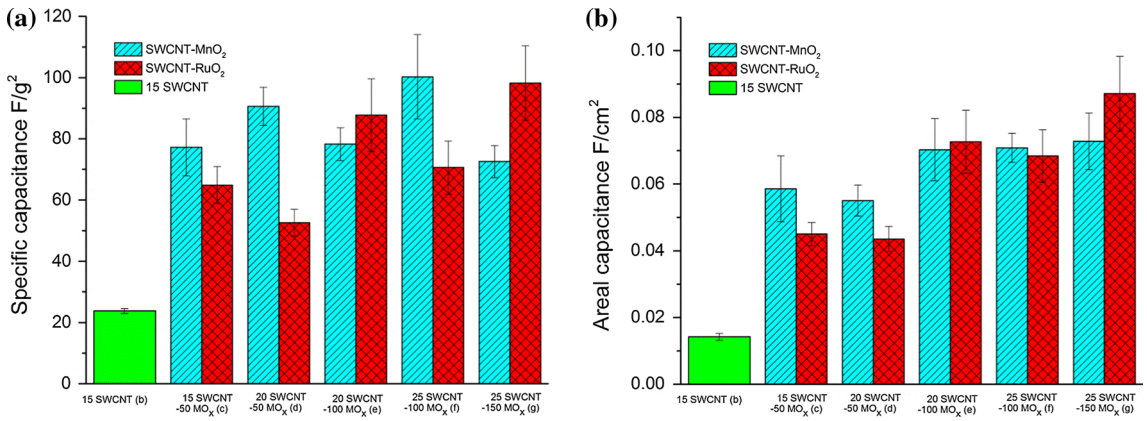

Fig. 3 **a** Specific and **b** areal capacitance of (*b*)–(*g*) layered samples as illustrated in Fig. 1. The SE of the mean was obtained by dividing the mean with the square root of the sample size ($n = 7$)

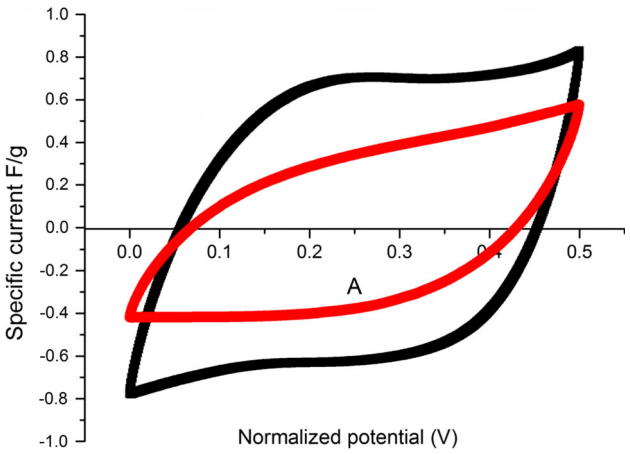

Fig. 4 CVs of SWCNT–RuO_2 (in *black*) and SWCNT–MnO_2 (in *red*). Scan rate: 5 mV/s (Color figure online)

Furthermore, SWCNT–MnO_2 discharges at a lower rate as compared to the SWCNT–RuO_2 (seen from the slope of the CV upon reversing the scan). The latter is presumably attributed to the higher conductivity of RuO_2 [23, 32].

Better insight to the SWCNT–MO_x-electrolyte interfaces can be obtained from EIS. Figure 5a shows the Nyquist diagrams of the SWCNT-only, SWCNT–RuO_2, and SWCNT–MnO_2 electrodes. Four segments, i.e., inductance, a semi-circle, Warburg diffusion and an incomplete arc, can be seen in each curve from high to low frequency. The high-frequency inductance is likely to be related to the porous nature of the electrodes (felts). The semi-circle at high frequency domain reflects the charge transfer resistance and the double-layer capacitance at the electrode/electrolyte interface. The Warburg diffusion in mid-frequency range is attributed to the diffusion of electrolyte in the active materials. The low-frequency incomplete arc may arise from the parallel of mass capacitance and leakage resistance [35, 36]. The data were fitted using the equivalent circuit illustrated in Fig. 5b, and selected parameters are shown in Table 1. The elements involved include the R_s, which mainly reflects the DC resistance of the film, C_{dl} which is the capacitance of the double layer, R_{ct} which is the charge transfer resistance, W, the Warburg element, R_L the leakage resistance, and C_L is the actual capacitance of the device. It can be seen that the R_s of the electrodes increases upon introducing the metal oxide. The resistance increase is likely due to the coverage of SWCNTs by metal oxides. The R_s is higher in the SWCNT–MnO_2 electrode than in the SWCNT–RuO_2, which is in agreement with the CV results (slope of charging/discharging). Furthermore, the R_{ct} and C_{dl} values for the SWCNT and SWCNT–RuO_2 samples are similar. This suggests that loading of RuO_2, unexpectedly, does not significantly affect electron transfer, which could be attributed to the increase of the surface area due to the porosity. The latter is confirmed by the morphology of the electrode surface as shown in FESEM (Fig. 6). On the other hand, the SWCNT–MnO_2 samples have higher R_{ct} and lower C_{dl}, probably related to the compactness of the MnO_2 films (Fig. 6). Moreover, the SWCNT–RuO_2 electrode has higher mass capacitance as compared with the SWCNT-only electrode, which is in agreement with the trend seen from CV results. Unfortunately reliable R_L and C_L values for the SWCNT–MnO_2 electrode could not be derived due to insufficient low-frequency data.

All these findings show that integrating the oxides with SWCNTs improves the capacitive performance of the electrodes, and in this context, the RuO_2 coatings perform better than the MnO_2. It is evident from Fig. 6 that the RuO_2 surface is smoother and more homogeneous than that of the MnO_2 but the typical pore sizes are much larger for RuO_2 as compared to the MnO_2 surfaces. Hence, the higher

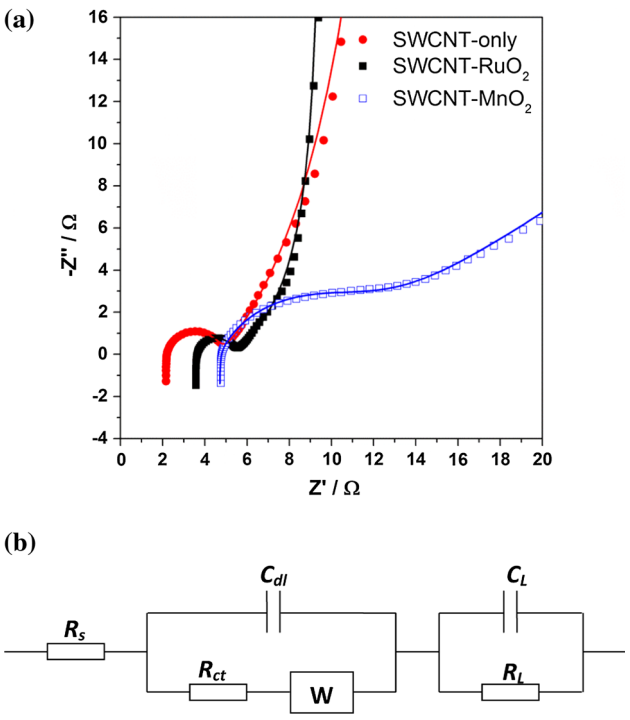

Fig. 5 **a** Electrochemical impedance spectroscopy of SWCNT-only, SWCNT–RuO_2, and SWCNT–MnO_2 devices measured at OCP in 1 M H_2SO_4 solution and **b** the equivalent circuit for fitting the data

Table 1 Selected EIS fitting results for the SWCNT-only, SWCNT–RuO_2, and SWCNT–MnO_2 samples

Sample	R_s (Ω)	R_{ct} (Ω)	C_{dl} (F)	R_L (Ω)	C_L (F)
SWCNT	2.16	2.532	2.27×10^{-4}	504	0.242
SWCNT–RuO_2	3.58	1.744	1.90×10^{-4}	253	0.498
SWCNT–MnO_2	4.78	7.495	9.20×10^{-4}	67	0.765

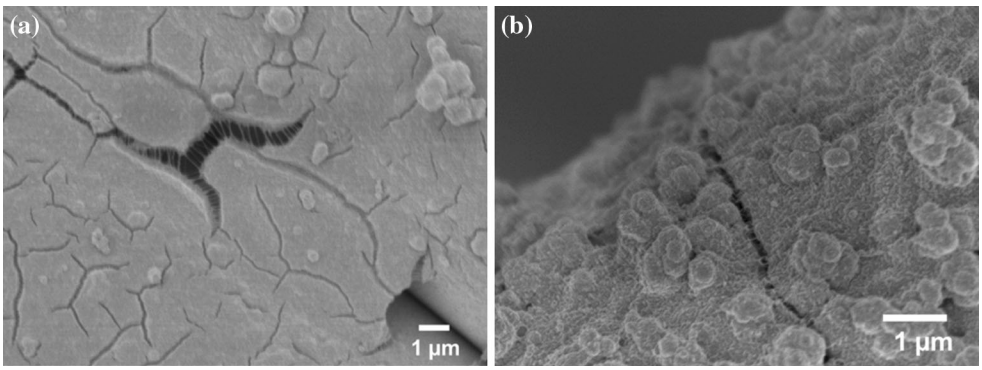

Fig. 6 FESEM showing microstructure of layered SWCNT–RuO_2 (**a**) and SWCNT–MnO_2 (**b**)

capacitance of the former may be attributed to the higher permeability of the RuO_2 layers.

To evaluate the cyclic capability of the pseudocapacitors, the capacitance retention was measured up to 1000 cycles. Figure 7 shows the change in the capacitance as a function of the number of charge/discharge cycles. The inset presents the individual charge/discharge at the 3rd, 500th, and 1000th cycle. While the capacitance of the SWCNT–MnO_2 shows a single significant decrease at approximately 300 cycles and remains more or less constant, that of SWCNT–RuO_2 decreased after 100 cycles and it declines continuously. After 1000 cycles, the SWCNT–MnO_2 sample retained 93 % of its original capacitance, while the SWCNT–RuO_2 sample retained only 86 %. This indicates that the SWCNT–MnO_2 electrodes have a higher cyclic stability as compared with the SWCNT–RuO_2 samples.

A comparison was also made between the layered (refer to (g) in Fig. 1) and the bulk deposited (refer to (i) in Fig. 1) samples. The latter was prepared by first soaking the glass fiber felt in the SWCNT solution (for 25 cycles) followed by electrodepositing the respective oxide (for 150 cycles). From Fig. 8, it can be seen that the layered samples improved more in terms of both specific and areal capacitances as compared to the bulk samples using the SWCNT-only samples as the baseline. Layering the deposition of SWCNTs and the oxides should increase the surface area of the oxide that is in contact with the SWCNTs hence maximizing the surface area of SWCNTs and oxides that is in contact with the electrolyte.

The performance of energy storage devices is commonly compared on a Ragone chart [37] where the specific energy is plotted versus the specific power. Figure 9 shows the Ragone plot where the performances of our electrodes are compared with commercial devices and some selected reports. This approach shows great promise in terms of the specific energy (4.14 and 4.25 Wh/kg for MnO_2–SWCNT and RuO_2–SWCNT devices, respectively, as compared to

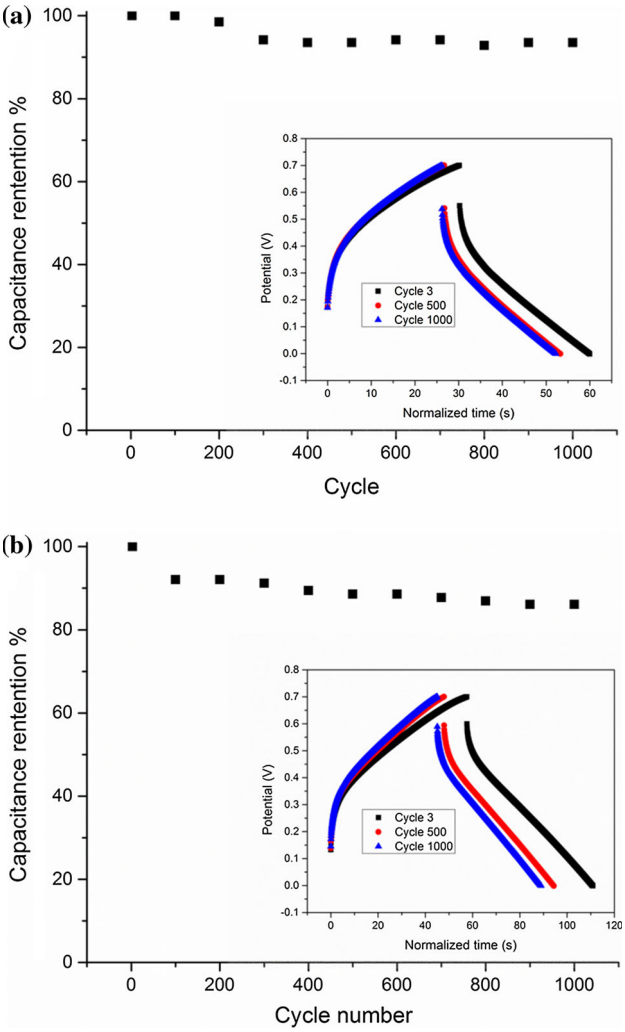

Fig. 7 Potential cycling showing capacitance retention of optimal **a** SWCNT–MnO_2 and **b** SWCNT–RuO_2 samples after 1000 cycles

2.35 and 3.60 Wh/kg for supercapacitors from Maxwell and Nesscap, respectively) taking into account that our system has not been fully optimized. Moreover, it should

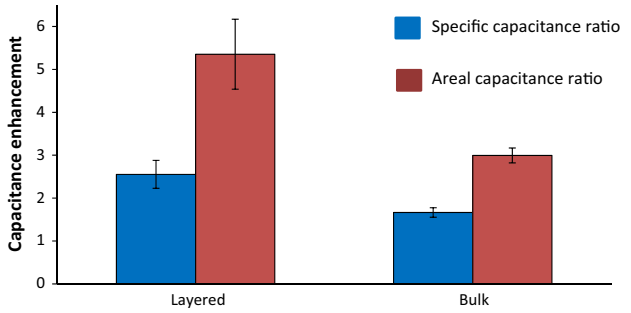

Fig. 8 Chart showing the improvement from SWCNT-only samples in both specific and areal capacitance for the layered and bulk samples after oxide deposition. The mean specific and areal capacitances of the CNT-oxide-layered samples were taken as a ratio to the mean specific and areal capacitances of the SWCNT-only samples to give the capacitance enhancement showing that the CNT-oxide-layered samples showed more specific and areal capacitance enhancement as compared to the bulk samples

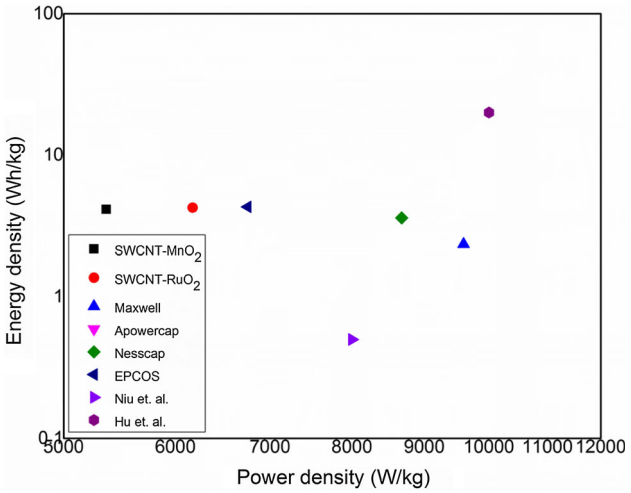

Fig. 9 Ragone plot of some commercial supercapacitors, recent reported values and the layered SWCNT–RuO_2 and SWCNT–MnO_2 samples [38, 39]

be noted that specific configuration of the glass fiber felt in our work results in high active surface area leading to high areal capacitance of the electrodes as compared to many other systems. This offers advantages in terms of practical applications such as printed flexible electronics and miniaturized capacitors.

Conclusions

In conclusion, the approach demonstrated in this study stems from the combination of an inert three-dimensional substrate that is coated by a conducting carbonaceous material and a redox oxide to form a layered structure. The inert substrate provides a low-cost porous network whereas the SWCNT provides the high conductivity and double-layer capacity which is well coupled with the high charge storage ability of the reversible redox oxides. Further improvement and optimization of this concept can be achieved by better control of the deposition parameters. This work has the potential to incorporate carbon nanomaterials into fabrics to be used as portable, wearable, and high-performance pseudocapacitors. The pseudocapacitors based on glass fiber felts can also be used to power electronic devices in harsh environments that involve high temperatures.

Acknowledgements This Research was conducted by NTU-HUJ-BGU Nanomaterials for Energy and Water Management Programme under the Campus for Research Excellence and Technological Enterprise (CREATE), which is supported by the National Research Foundation, Prime Minister's Office, Singapore.

References

1. Hughes M, Shaffer MSP, Renouf AC, Singh C, Chen GZ, Fray DJ, Windle AH (2002) Electrochemical capacitance of nanocomposite films formed by coating aligned arrays of carbon nanotubes with polypyrrole. Adv Mater 14(5):382–385. doi:10.1002/1521-4095(20020304)14:5<382:aid-adma382>3.0.co;2-y
2. Khomenko V, Frackowiak E, Beguin F (2005) Determination of the specific capacitance of conducting polymer/nanotubes composite electrodes using different cell configurations. Electrochim Acta 50(12):2499–2506. doi:10.1016/j.electacta.2004.10.078
3. Lee H, Kim H, Cho MS, Choi J, Lee Y (2011) Fabrication of polypyrrole (PPy)/carbon nanotube (CNT) composite electrode on ceramic fabric for supercapacitor applications. Electrochim Acta 56(22):7460–7466. doi:10.1016/j.electacta.2011.06.113
4. Li J, Xie H, Li Y, Liu J, Li Z (2011) Electrochemical properties of graphene nanosheets/polyaniline nanofibers composites as electrode for supercapacitors. J Power Sources 196(24):10775–10781. doi:10.1016/j.jpowsour.2011.08.105
5. Ting W, Kiebele A, Ma J, Mhaisalkar S, Gruner G (2011) Charge transfer between polyaniline and carbon nanotubes supercapacitors: improving both energy and power densities. J Electrochem Soc 158(1):A1–A5. doi:10.1149/1.3505994
6. Zhong-Shuai W, Da-Wei W, Wencai R, Jinping Z, Guangmin Z, Feng L, Hui-Ming C (2010) Anchoring hydrous RuO_2 on graphene sheets for high-performance electrochemical capacitors. Adv Func Mater 20(20):3595–3602. doi:10.1002/adfm.201001054
7. Kim I-H, Kim J-H, Kim K-B (2005) Electrochemical characterization of electrochemically prepared ruthenium oxide/carbon nanotube electrode for supercapacitor application. Electrochem Solid-State Lett 8(7):A369–A372. doi:10.1149/1.1925067
8. Dandan Z, Zhi Y, Liying Z, Xinliang F, Yafei Z (2011) Electrodeposited manganese oxide on nickel foam-supported carbon nanotubes for electrode of supercapacitors. Electrochem Solid-State Lett 14(6):93–96. doi:10.1149/1.3562927
9. Yuan L, Lu X-H, Xiao X, Zhai T, Dai J, Zhang F, Hu B, Wang X, Gong L, Chen J, Hu C, Tong Y, Zhou J, Wang ZL (2012) Flexible solid-state supercapacitors based on carbon nanoparticles/MnO_2 nanorods hybrid structure. ACS Nano 6(1):656–661. doi:10.1021/nn2041279
10. Chen Z, Augustyn V, Wen J, Zhang Y, Shen M, Dunn B, Lu Y (2011) High-performance supercapacitors based on intertwined CNT/V_2O_5 nanowire nanocomposites. Adv Mater 23(6):791–795. doi:10.1002/adma.201003658

11. Peng C, Zhang S, Jewell D, Chen GZ (2008) Carbon nanotube and conducting polymer composites for supercapacitors. Prog Nat Sci 18(7):777–788. doi:10.1016/j.pnsc.2008.03.002
12. de las Casas C, Li W (2012) A review of application of carbon nanotubes for lithium ion battery anode material. J Power Sources 208:74–85. doi:10.1016/j.jpowsour.2012.02.013
13. Peigney A, Laurent C, Flahaut E, Bacsa RR, Rousset A (2001) Specific surface area of carbon nanotubes and bundles of carbon nanotubes. Carbon 39(4):507–514
14. Parkash S (1974) Adsorption of weak and non-electrolytes by activated carbon. Carbon 12(1):37–43. doi:10.1016/0008-6223(74)90038-4
15. Liu K, Sun Y, Zhou R, Zhu H, Wang J, Liu L, Fan S, Jiang K (2010) Carbon nanotube yarns with high tensile strength made by a twisting and shrinking method. Nanotechnology 21(4):045708. doi:10.1088/0957-4484/21/4/045708
16. Bose S, Kuila T, Mishra AK, Rajasekar R, Kim NH, Lee JH (2012) Carbon-based nanostructured materials and their composites as supercapacitor electrodes. J Mater Chem 22(3):767–784. doi:10.1039/c1jm14468e
17. Pan H, Li J, Feng YP (2010) Carbon nanotubes for supercapacitor. Nanoscale Res Lett 5(3):654–668. doi:10.1007/s11671-009-9508-2
18. Liu X, Pickup PG (2011) Carbon fabric supported manganese and ruthenium oxide thin films for supercapacitors. J Electrochem Soc 158(3):A241–A249. doi:10.1149/1.3525591
19. Park JH, Ko JM, Park OO (2003) Carbon nanotube/RuO_2 nanocomposite electrodes for supercapacitors. J Electrochem Soc 150(7):A864–A867. doi:10.1149/1.1576222
20. Kim Y-T, Tadai K, Mitani T (2005) Highly dispersed ruthenium oxide nanoparticles on carboxylated carbon nanotubes for supercapacitor electrode materials. J Mater Chem 15(46):4914–4921. doi:10.1039/b511869g
21. Hsieh T-F, Chuang C-C, Chen W-J, Huang J-H, Chen W-T, Shu C-M (2012) Hydrous ruthenium dioxide/multi-walled carbon-nanotube/titanium electrodes for supercapacitors. Carbon 50(5):1740–1747. doi:10.1016/j.carbon.2011.12.017
22. Kim I-H, Kim J-H, Lee Y-H, Kim K-B (2005) Synthesis and characterization of electrochemically prepared ruthenium oxide on carbon nanotube film substrate for supercapacitor applications. J Electrochem Soc 152(11):A2170–A2178. doi:10.1149/1.2041147
23. Hou Y, Cheng Y, Hobson T, Liu J (2010) Design and synthesis of hierarchical MnO_2 nanospheres/carbon nanotubes/conducting polymer ternary composite for high performance electrochemical electrodes. Nano Lett 10(7):2727–2733. doi:10.1021/nl101723g
24. Sang-Bok M, Kyung-Wan N, Won-Sub Y, Xiao-Qing Y, Kyun-Young A, Ki-Hwan O, Kwang-Bum K (2008) Electrochemical properties of manganese oxide coated onto carbon nanotubes for energy-storage applications. J Power Sources 178(1):483–489. doi:10.1016/j.jpowsour.2007.12.027
25. Amade R, Jover E, Caglar B, Mutlu T, Bertran E (2011) Optimization of MnO_2/vertically aligned carbon nanotube composite for supercapacitor application. J Power Sources 196(13):5779–5783. doi:10.1016/j.jpowsour.2011.02.029
26. Wang W, Guo S, Lee I, Ahmed K, Zhong J, Favors Z, Zaera F, Ozkan M, Ozkan CS (2014) Hydrous ruthenium oxide nanoparticles anchored to graphene and carbon nanotube hybrid foam for supercapacitors. Sci Rep. doi:10.1038/srep04452
27. Portet C, Taberna PL, Simon P, Flahaut E, Laberty-Robert C (2005) High power density electrodes for carbon supercapacitor applications. Electrochim Acta 50(20):4174–4181. doi:10.1016/j.electacta.2005.01.038
28. Moore JJ, Kang JH, Wen JZ (2012) Fabrication and characterization of single walled nanotube supercapacitor electrodes with uniform pores using electrophoretic deposition. Mater Chem Phys 134(1):68–73. doi:10.1016/j.matchemphys.2012.02.030
29. Girishkumar G, Rettker M, Underhile R, Binz D, Vinodgopal K, McGinn P, Kamat P (2005) Single-wall carbon nanotube-based proton exchange membrane assembly for hydrogen fuel cells. Langmuir 21(18):8487–8494. doi:10.1021/la051499j
30. Yu D, Dai L (2010) Self-assembled graphene/carbon nanotube hybrid films for supercapacitors. J Phys Chem Lett 1(2):467–470
31. Il-Hwan K, Jae-Hong K, Kwang-Bum K (2005) Electrochemical characterization of electrochemically prepared ruthenium oxide/carbon nanotube electrode for supercapacitor application. Electrochem Solid-State Lett 8(7):369–372. doi:10.1149/1.1925067
32. Lv P, Zhang P, Feng Y, Li Y, Feng W (2012) High-performance electrochemical capacitors using electrodeposited MnO_2 on carbon nanotube array grown on carbon fabric. Electrochim Acta 78:515–523. doi:10.1016/j.electacta.2012.06.085
33. Rakhi RB, Cha D, Chen W, Alshareef HN (2011) Electrochemical energy storage devices using electrodes incorporating carbon nanocoils and metal oxides nanoparticles. J Phys Chem C 115(29):14392–14399. doi:10.1021/jp202519e
34. Yu G, Hu L, Vosgueritchian M, Wang H, Xie X, McDonough JR, Cui X, Cui Y, Bao Z (2011) Solution-processed graphene/MnO_2 nanostructured textiles for high-performance electrochemical capacitors. Nano Lett 11(7):2905–2911. doi:10.1021/nl2013828
35. Masarapu C, Zeng HF, Hung KH, Wei B (2009) Effect of temperature on the capacitance of carbon nanotube supercapacitors. ACS Nano 3(8):2199–2206. doi:10.1021/nn900500n
36. Hastak RS, Sivaraman P, Potphode DD, Shashidhara K, Samui AB (2012) All solid supercapacitor based on activated carbon and poly [2,5-benzimidazole] for high temperature application. Electrochim Acta 59:296–303. doi:10.1016/j.electacta.2011.10.102
37. Dileo RA, Castiglia A, Ganter MJ, Rogers RE, Cress CD, Raffaelle RP, Landi BJ (2010) Enhanced capacity and rate capability of carbon nanotube based anodes with titanium contacts for lithium ion batteries. ACS Nano 4(10):6121–6131. doi:10.1021/nn1018494
38. Niu C, Sichel EK, Hoch R, Moy D, Tennent H (1997) High power electrochemical capacitors based on carbon nanotube electrodes. Appl Phys Lett 70(11):1480–1482. doi:10.1063/1.118568
39. Hu L, Pasta M, Mantia FL, Cui L, Jeong S, Deshazer HD, Choi JW, Han SM, Cui Y (2010) Stretchable, porous and conductive energy textiles. Nano Lett 10(2):708–714. doi:10.1021/nl903949m